RECENT PHYSICS RESULTS FROM THE
CERN $\bar{p}p$ COLLIDER

J. Rohlf

CERN, Geneva, Switzerland
and
Harvard University, Cambridge, MA 02138

Summary

Recent physics results from the UA1 experiment at the CERN SPS Collider are presented.[1] Some new results on jet production are given, as well as latest results on W and Z^0 production.[2] A comparison between UA1 and UA2 results concerning the intermediate vector boson masses is made.

Jets

The first striking result from $\bar{p}p$ collisions at a center-of-mass energy of 540 GeV is that if we trigger on high global transverse energy, the events are dominated by jets.[3] These jets are particularly distinctive (separated from soft hadronic background) for transverse momenta greater than about 10 GeV. Most of the events with high global transverse momentum are two-jet events. However, a few percent of these events contain a visable third jet and some events are observed with 4, 5, or even 6 jets (Fig. 1).

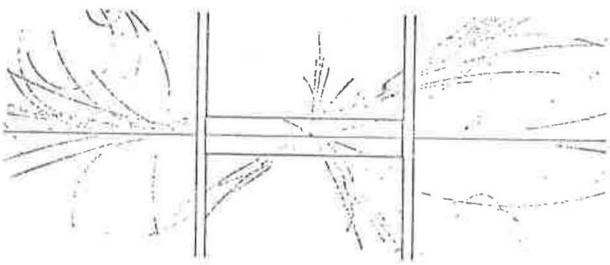

Fig. 1. UA1 multi-jet event as observed in the central tracking chambers.

The multi-jet mass distribution, which is dominated by two-jet events, is shown in Fig. 2. The data are from 15 nb^{-1} integrated luminosity. Events are observed with invariant mass in excess of 250 GeV. This exceeds the energy available even for LEP Phase II! Of course, the typical collision does not contain such high-mass jets; the events of Fig. 2 come from a sample of about 10^9 collisions. However, the signature of these events is very clean and they are very easy to trigger on (in hardware) and select in the offline analysis.

We may probe the structure of the proton with a parton from the antiproton, or vice versa, analogous to the case of lepton-nucleon scattering. Here, the probe is a quark or a gluon instead of a lepton. The state we observe in the laboratory is one of two jets. We have an uncertainty in knowledge of the momentum transfer squared (q^2) of the scattering process, but it is of order $q^2 \sim p_T{}^2 = 1200$ GeV^2, where p_T is the transverse momentum of each jet. These data are shown in Fig. 3 where we plot the proton and antiproton structure function F(x). This function tells the relative probability of finding a quark or gluon in the proton with momentum fraction x, sampled at q^2 momentum tranfer squared. This is a much higher q^2 than achieved before in any other hard scattering process.

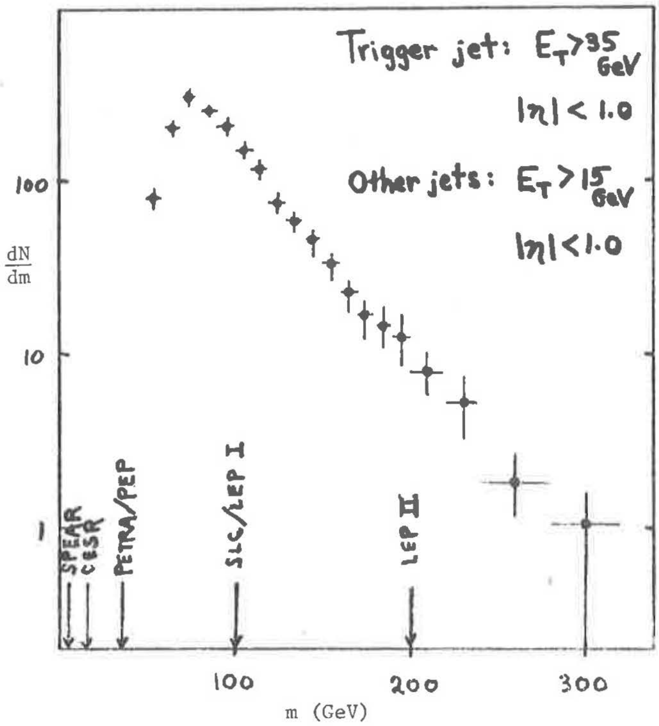

Fig. 2. Jet yield, dN/dm, where m is the multi-jet mass. The data are from 15 nb^{-1}.

We may make a rough comparison with data from νN scattering from the CDHS experiment, at a q^2 of 2-200 GeV^2. A scaling of these data with q^2 as expected from QCD produces rough agreement between the experiments. The essential point here is that we are using a new process, quark and gluon scattering, to extend the proton structure measurements into a new kinematic region.

W Production

I now turn to the main part of my presentation, which is the subject of the intermediate vector bosons, W and Z^0. We demonstrated in the first W publication (6 events) that selection of an isolated high transverse momentum electron with no coplanar jet within 30 degrees, gave events which also has missing transverse energy approximately equal and opposite to that of the electron.[4] The electron selection is a straightforward set of cuts which select an isolated high momentum charged track from the central drift chamber which is geometrically matched with an electromagnetic

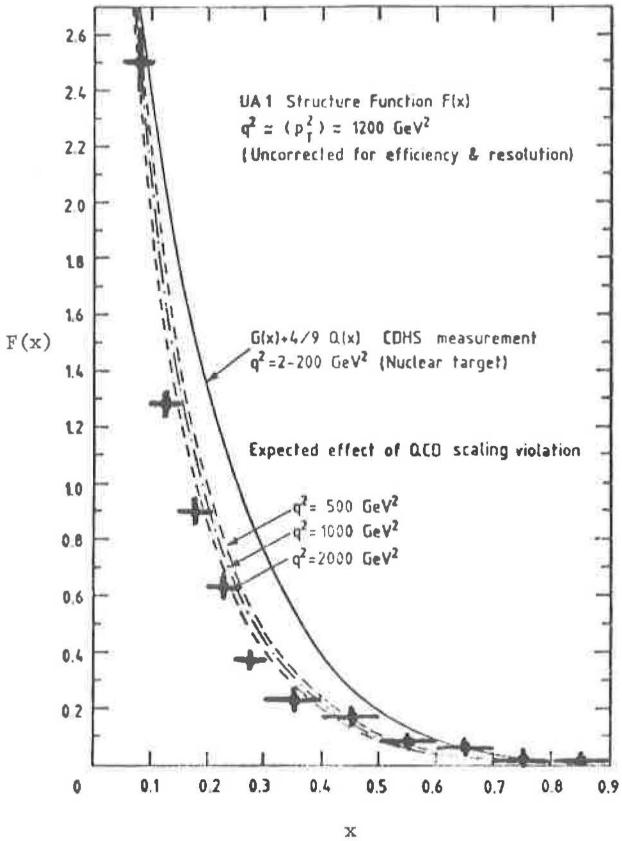

Fig. 3. Proton structure function, F(x), derived from high transverse momentum 2-jet events, assumed to arise from quark or gluon hard scatterings.

calorimeter shower.[4] We veto events which have a coplanar jet within 30 degrees.[5] For these events we make a scatter-plot (Fig. 4) of the electron transverse energy vs. the missing (ν) transverse energy

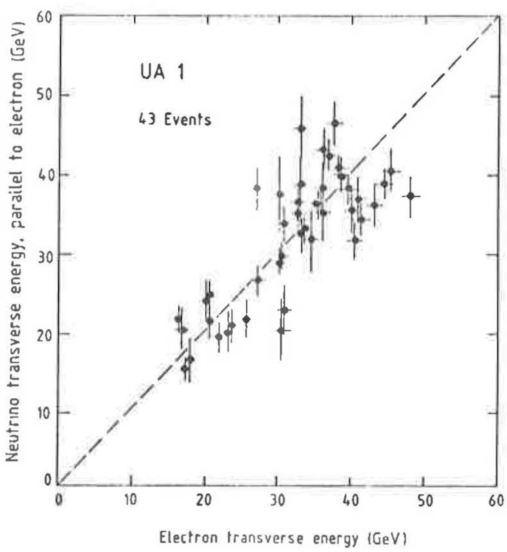

Fig. 4. Scatter-plot of electron transverse energy vs. missing transverse energy (parallel to electron).

parallel to the electron. We see that these events with large electron transverse energy, $E_T > 15$ GeV are accompanied by a large missing E_T. This missing E_T is approximately equal in magnitude to the electron E_T, indicating a two-body final state, eν. The electron and neutrino are back-to-back (coplanar with the beam axis) in the transverse plane as shown in Fig. 5. The overall activity of these events is very "mimimum bias-like" and they therefore have a striking signature.

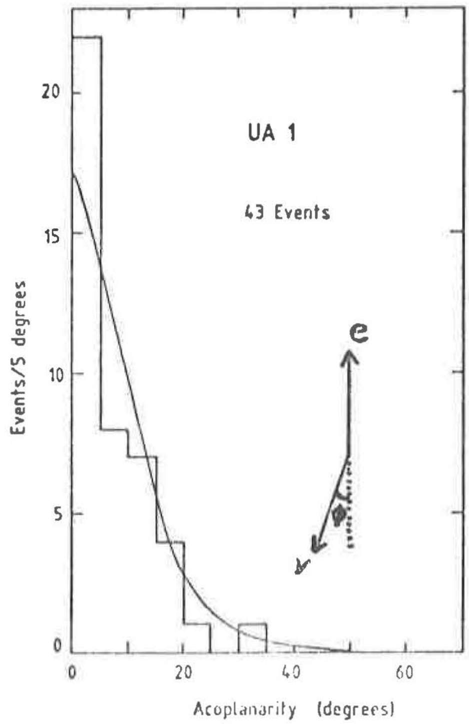

Fig. 5. Angle of the ν with respect to the plane containing the electron and the beam axis. The curve is the Monte Carlo expectation based on QCD effects which give the W some transverse momentum.

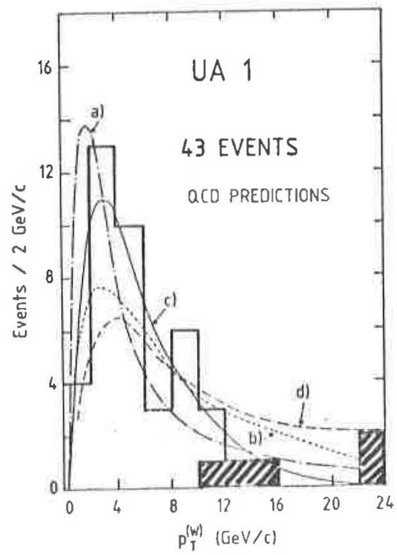

Fig. 6. Measured W transverse momentum. The curves are various calculations: a) lowest order QCD, b) Halzen et al., c) Aurenche et al., d) Nakamura et al.[6] The shaded events have a visible jet ($p_T > 10$ GeV).

The W transverse momentum is measured directly; it is the vector sum of the electron and neutrino transverse momentum. This is shown in Fig. 6. It agrees fairly well with predictions based on QCD.[6]

To determine the mass of the W, we introduce a variable called transverse mass[4] (Fig. 7) defined as $m_T = 2 E_T^e E_T^\nu (1 - \cos \Delta\phi)$, where $\Delta\phi$ is the angle between the e and the ν in the transverse plane. The

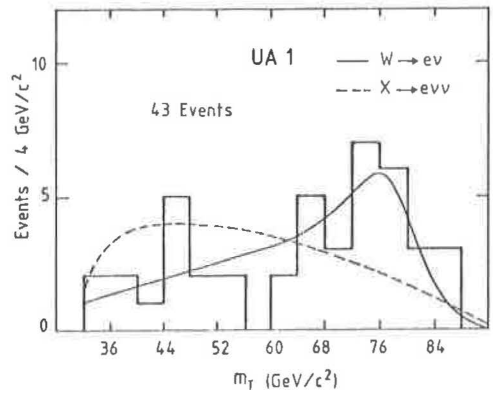

Fig. 7. Measured transverse mass distribution (histogram) along with expectation for $W \to e\nu$ with m_W = 80 GeV (solid curve) and 3-body decay $X \to e\nu\nu$ (dashed curve).

true W mass is always greater than or equal to m_T, apart from the effects of experimental resolution. We may use two-body decay kinematics of W decay and experimental resolution of the shower counters to relate the observed m_T spectrum to the desired quantity, m_W. A maximum likelihood fit gives a value for the W mass of 80.9 ± 1.5 GeV (± 2.4 GeV systematic error due to shower counter calibration). We also find a limit on the width of the W from this fit to be $\Gamma_W < 7$ GeV at 90% C.L. These fits are not sensitive to the assumed angular distribution of the W decay, the W transverse momentum, or the W longitudinal momentum distributions. We are not able to simultaneously fit the missing E_T, the electron E_T, and the transverse mass distributions to a 3-body decay into an electron and two neutrinos for any assumed mass. The dashed curve in Fig. 7, for example, is the best fit to the high transverse momentum electron and neutrino events for a 3-body decay, but it cannot fit the transverse mass distribution.

Given the 6 measured quantities p_x, p_y, and p_z of the electron, and p_y and p_z (transverse momentum components) of the neutrino, and the fit to the W mass, there exist two possible solutions for the longitudinal momentum (p_x) of the neutrino. However, most of the time one of the solutions is forbidden by conservation of energy and momentum. This is shown in Fig. 8, where we plot the W longitudinal momentum fraction (which is the sum of the electron and neutrino longitudinal momenta) of the beam energy, 270 GeV. The shaded part indicates those events which have unambiguous solutions for the neutrino longitudinal momentum. The remaining events are plotted as the lower of the two x-solutions. The low-x solution of these few ambiguous events agrees with the unambiguous solutions (see Fig. 8). The solid curve of Fig. 8 is that expected from quark-antiquark annihilation with u quark distributions of $(1-x)^3$ and d quark distributions of $(1-x)^4$, as indicated from other experiments.

We may go to the center-of-mass of the colliding

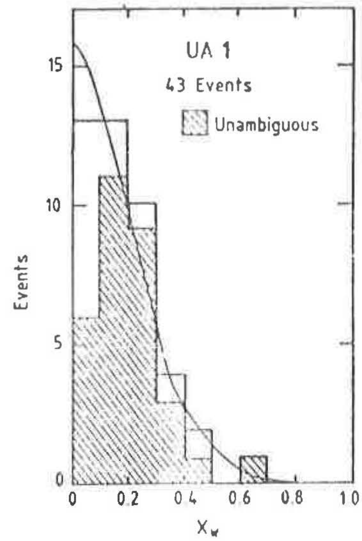

Fig. 8. W longitudinal momentum distribution, normalized to the beam energies of 270 GeV. Most events have an unambiguous solution (shaded events), see text.

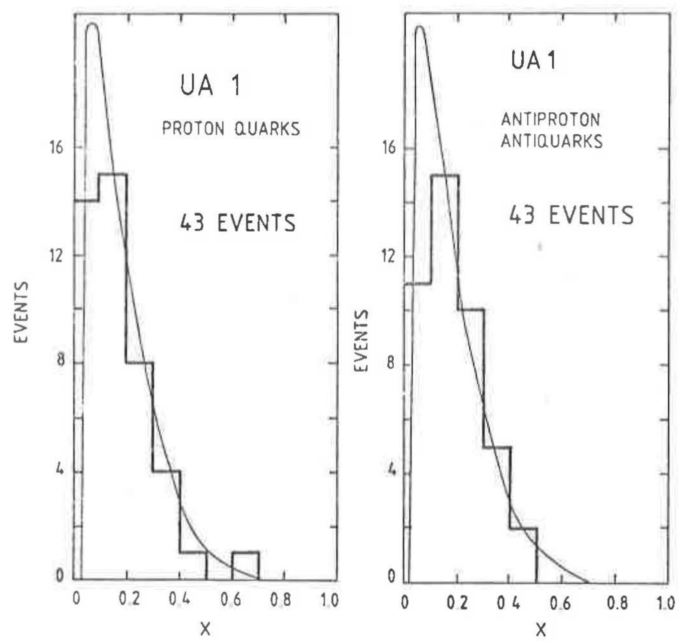

Fig. 9. a) Quark momenta (u or d) , normalized to 270 GeV, which make W's; b) same for antiquarks ($\bar{u}$ or $\bar{d}$) which make W's.

partons with the following relations: $x_1 x_2 \propto m_W^2$ and $x_1 - x_2 = x_W$, where x_1 and x_2 are the momentum fractions of the quark and antiquark which produce the W. Fig. 9 a) shows the x distribution for quarks originating from the proton and Fig. 9 b) shows the same x distribution for the antiquarks from the antiproton. Instead of separating these parton x distributions by matter and antimatter, we may separate them by quark flavor. These x distributions are shown in

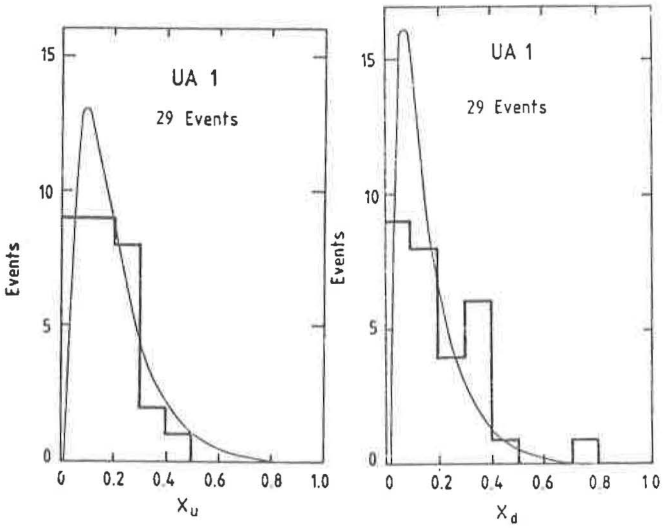

Fig. 10. a) u and $\bar{u}$ flavored quark momenta which make W's; b) d and $\bar{d}$ flavored quark momenta which make W's.

Fig. 10 for u and $\bar{u}$ quarks (a) and for d and $\bar{d}$ quarks (b). The solid curves in Figs. 9 and 10 are the simple expectations for u and d distributions of $(1-x)^3$ and $(1-x)^4$, respectively, when sampled at the W pole. Within the available statistics, we observe no difference in the quark distributions of u, $\bar{u}$, d, or $\bar{d}$ when sampled at the W mass.

W Decay

W's are expected to be fully polarized when produced in quark-antiquark annihilations as depicted in Fig. 11. When the W decays, the electron "remembers" the directions of the original quarks and antiquarks. In the W rest frame, the angular distribution of the

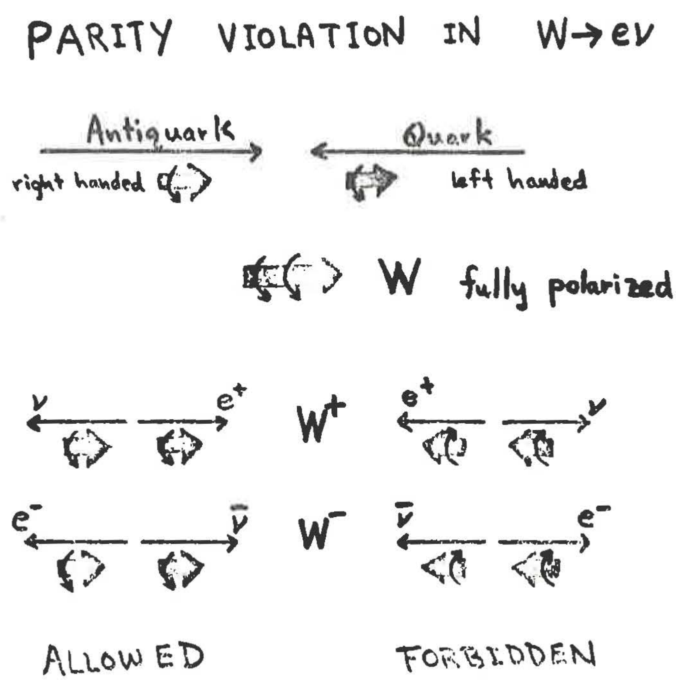

Fig. 11. Diagram showing W polarization at production and allowed and suppressed decays.

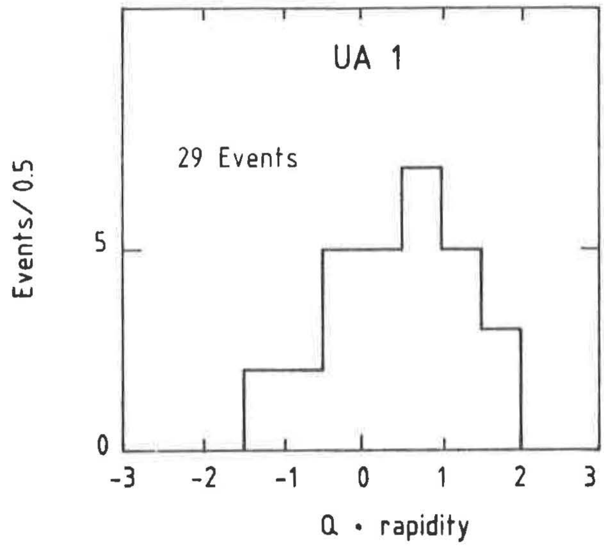

Fig. 12. Electric charge times rapidity (in the laboratory frame) for W events. Positive rapidity is defined as the direction of the outgoing antiproton beam.

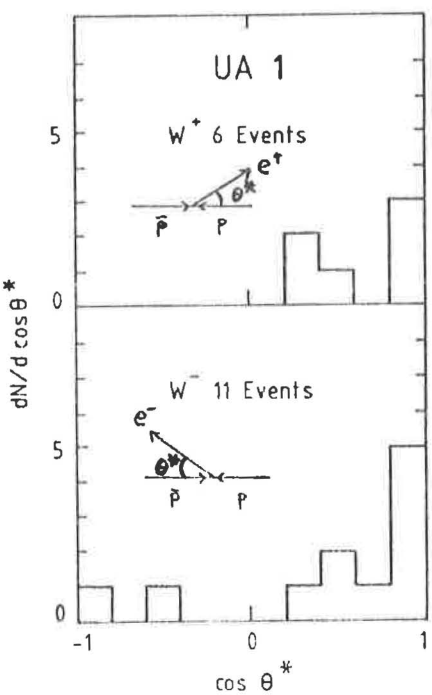

Fig. 13. Uncorrected angular distributions in the rest frame of the W for events which have unambiguous solutions for the neutrino momentum for a) W^+ decays and b) W^- decays. Note that the definition of cos θ^* is reversed in a) and b).

electron with respect to the outgoing proton is expected to be $(1 + \cos\theta^*)^2$. The longitudinal momentum of the W smears this distribution in the laboratory ($\bar{p}p$) frame. However, we have shown from the quark x-distributions that this smearing has no prefered direction; that is, quarks in the proton have the same structure function as antiquarks in the antiproton. In the $\bar{p}p$ frame we may observe the asymmetry in W decay by plotting charge times rapidity, $Q \cdot y$, (Fig. 12) where the rapidity sign is defined as positive (negative) for the proton (antiproton) direction.

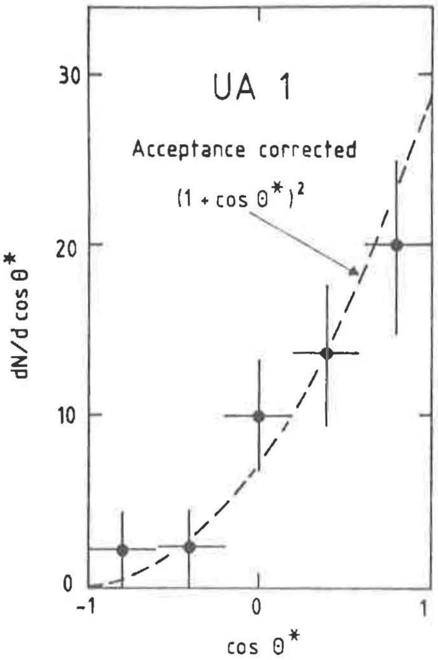

Fig. 14. Acceptance corrected angular distribution observed in the rest frame of the W.

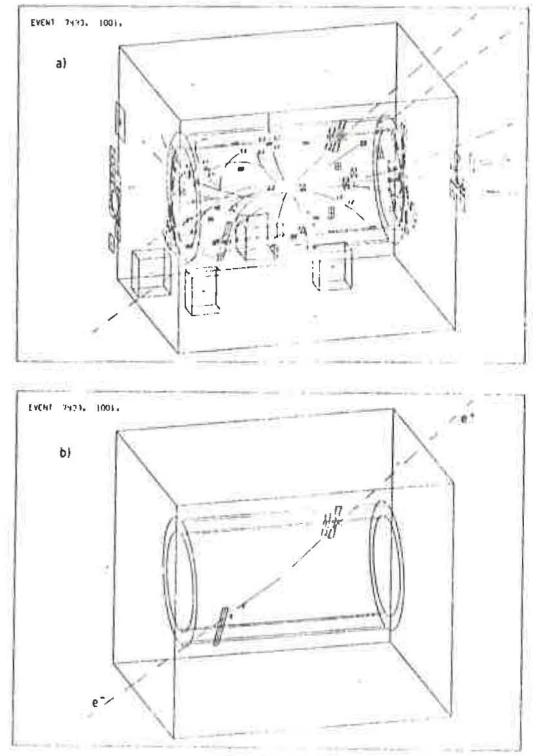

Fig. 15. Graphics display of Z^0 event where a) all tracks and calorimeter hits are displayed, and b) only those calorimeter hits and tracks with transverse energy greater than 2 GeV are displayed.

If we transform to the rest frame of the W (which we may only do for unambiguous events), we see a clear asymmetry in the uncorrected angular distributions for $W^+ \rightarrow e^+\nu$ (Fig. 13 a) and $W^- \rightarrow e^-\nu$ (Fig. 13 b). Using the fact that the apparatus is symmetric in cos θ , we may use the data to correct bin-by-bin for the acceptance of the unambiguous-neutrino selection. We have an additional correction of about 30% in the last bins for the transverse momentum cut on the electron. This fully corrected distribution is shown in Fig. 14, along with the simple expectation of $(1 + \cos\theta^*)^2$. We see three things from these data in Fig. 14: 1) parity is clearly violated, 2) the dominant production mechanism is quark-antiquark annihilation by valence quarks (full polarization at production), and 3) the preferred spin assignment of the W particle is 1. If either 2) or 3) were not true, we would expect strong deviations from the dashed curve of Fig. 14; in particular, we would get an excess of events at $\cos\theta^* = -1$. In fact, the one event observed at $\cos\theta^*$ near -1 could be due to a small component of sea-quark contribution to W production.

The measured cross section times branching ratio for $\bar{p}p \rightarrow W + X \rightarrow e + \nu + X$ is 0.53 ± 0.08 nb (± 0.09 nb systematic error). This is in good agreement with the theoretical prediction of 0.39 nb.[7]

Z^0 Production and Decay

If instead of selecting one electron with a coplanar jet veto, we select two electrons, then[8] we find events such as the one shown in Fig. 15. Part a) of Fig. 15 shows all struck calorimeter cells (boxes) as well as all charged tracks. However, if we make a modest threshold cut of 2 GeV transverse momentum (Fig. 15 b), only two tracks of high momentum and two showers of high energy (approximately 50 GeV each) remain. We find 4 such high mass e^+e^- pairs. The transverse energy flow in these events is shown in Fig. 16.

If we select events with two muons instead of two electrons, we find events as shown in Fig. 17.

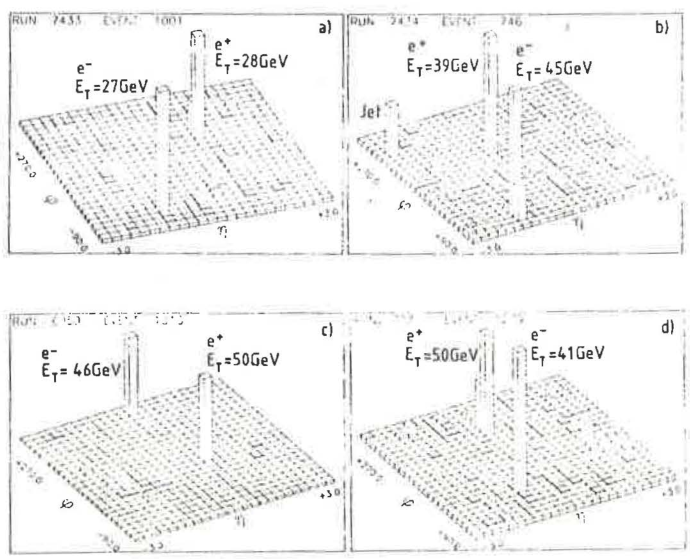

Fig. 16. Transverse energy flow in the electromagnetic calorimeters for the 4 high-mass e^+e^- events.

A summary of the dilepton analysis is shown in Fig. 18. Here we show the invariant mass of all dileptons observed. We find 5 dimuon events clustered near the 15 GeV muon-pair threshold and 1 dielectron event near the 30 GeV electron-pair threshold. We interpret these lower mass events to be most likely due to the Drell-Yan mechanism. We find no events

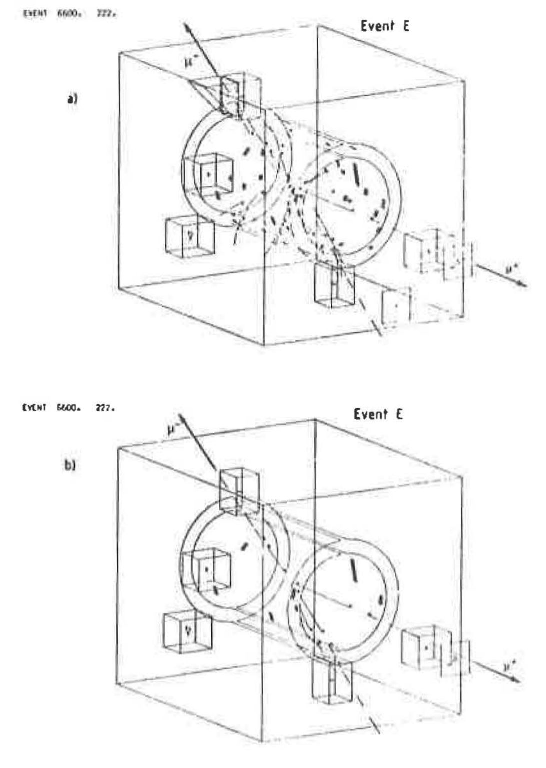

Fig. 17. $Z^0 \rightarrow \mu^+\mu^-$ event: a) all tracks and calorimeter hits, and b) those tracks and hits with transverse energy greater than 2 GeV. A significant jet with a p_T of about 25 GeV is observed in this event which balances the p_T of the dimuon system.

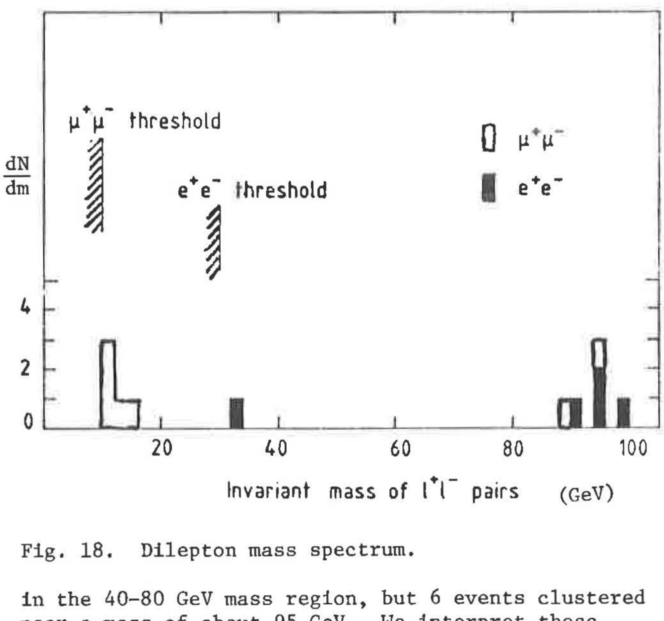

Fig. 18. Dilepton mass spectrum.

in the 40-80 GeV mass region, but 6 events clustered near a mass of about 95 GeV. We interpret these events as being due to the Z^0 resonance and fit a mass of 95.6 ± 1.4 GeV (± 3 GeV systematic error) and an upper limit on the width (Breit-Wigner) of $\Gamma < 8.5$ GeV (full-width) at 90% C.L. We measure a production cross section times branching ratio into e^+e^- of 49 ± 22 ± 8 pb.

Figure 19 shows a plot of W mass vs. Z^0 mass. The eliptical shape of the confidence level contours reflects the systematic error in the energy scale which effects both the W and Z^0 masses. We see that

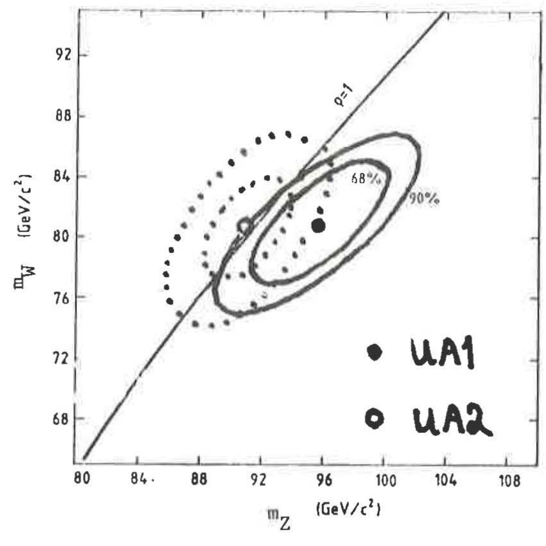

Fig. 19. Measured W and Z^0 masses with 68% and 90% C.L. contours.

we are just compatible with the standard model predictions of $\rho = 1$. Also shown here are the results of UA2 who find a similar W mass but a somewhat smaller Z^0 mass.[9] At this stage, the results are fully compatible with each other (UA1 and UA2) and with the minimal standard model.

Number of Neutrino Species

The direct limit on the width of the Z^0 (less than 8.5 GeV at 90% C.L.) limits the number of neutrino species to about 30. This is because the expected Z^0 width is 3 GeV for 3 neutrino species and each new family increases the Z^0 width by about 180 MeV. We may try to do somewhat better on this limit by taking into account the cross section measurements also. There is clearly some information here since if there were an infinite number of neutrinos, we

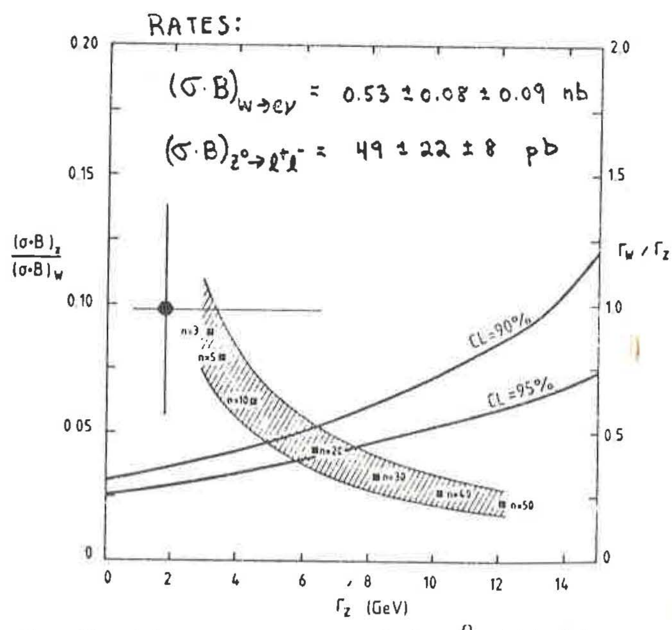

Fig. 20. Direct measurement of the Z^0 width (abscissa) plotted against the ratio of W to Z^0 widths extracted from cross section measurements (ordinate).

could not have observed the 6 events because the partial rate into dileptons would be negligible. By using the relations,

$$(\sigma \cdot B)_Z = \sigma_Z \cdot \Gamma_{ee} / \Gamma_{all} \quad \text{and}$$

$$(\sigma \cdot B)_W = \sigma_W \cdot \Gamma_{l\nu} / \Gamma_{all} ,$$

we may convert the ratio of $(\sigma \cdot B)_Z / (\sigma \cdot B)_W$ to a ratio of full widths provided that we can predict the ratio of cross sections σ_W / σ_Z . The partial widths are well predicted by theory. The W cross section was predicted absolutely to about 20% (before the experiment!) and the ratio of cross sections should be easier to predict because some terms in the calculation cancel. Putting in the theoretical predictions of Paige[7] for the W to Z^0 total cross section ratio, we may convert the the ratio of cross section times branching ratios to a ratio of total widths, Γ_W / Γ_Z . This is shown in Fig. 20. The directly measured quantity (ratio of cross section times branching ratio for the W and Z^0) is plotted vs. the directly measured width, Γ_Z. Using the total cross section ratio from Paige, we obtain the right-hand axis Γ_W / Γ_Z . We then indicate where we expect the measured point to lie for n = 3, 5, 10 , 20 ... families of neutrinos. (This is because more neutrino species increase Γ_Z but not Γ_W .) The hatched region indicates the 20% uncertainty in knowledge of σ_W / σ_Z . We thus improve the limit to $n < 15$ neutrino families at 90% C.L. Of course, this method can be made more precise when the total W and Z^0 cross sections are measured directly from the quark (jet) decay modes.[10]

References and Footnotes

1. UA1 Collaboration: Aachen, Annecy (LAPP), Birmingham, CERN, Helsinki, Queen Mary College (London), College de France (Paris), U. C. Riverside, Rome, Rutherford, Saclay (CEN), Vienna.

2. The UA1 detector is not discussed in this talk but is described by B. Sadoulet (this conference).

3. M. Banner et al., Phys. Lett. 118B, 203 (1982); G. Arnison et al., Phys. Lett. 123B, 115 (1982). See also G. Arnison et al., CERN preprints EP/83-118 and EP/83-119 (1983).

4. G. Arnison et al., Phys. Lett. 122B, 103 (1983). See also M. Banner et al., Phys. Lett. 122B, 476 (1983).

5. The events with an electron and a coplanar jet are not understood at this time. However, we note that these events do not have large missing energy as do the W events (see Ref. 4).

6. F. Halzen et al., Phys. Lett. 78B, 318 (1978); P. Aurenche et al., Annecy preprint LAPP-TH-78 (1983); A. Nakamura et al., Frascati preprint INF-83/43 (1983).

7. F. Paige et al., BNL 29777 (1981).

8. G. Arnison et al., Phys. Lett. 126B, 398 (1983).

9. UA2 Collaboration, results reported at the Brighton Conference, Brighton, U.K. (1983).

10. See N. Cabbibo, Third Topical Workshop on Proton Antiproton Collider Physics, Rome (1983).